

# Modeling the response of HCP polycrystals deforming by slip and twinning using a finite element representation of the orientation space

Babak Kouchmeshky and Nicholas Zabaras<sup>\*</sup>

*Materials Process Design and Control Laboratory, Sibley School of Mechanical and Aerospace Engineering, 101 Frank H. T. Rhodes Hall, Cornell University, Ithaca, NY 14853-3801, USA*

---

## Abstract

A continuum approach is presented for predicting the constitutive response of HCP polycrystals using a simple non-hardening constitutive model incorporating both slip and twinning. This has been achieved by considering a physically based methodology for restricting the amount of the twinning activity. A continuum approach is used in modeling the texture evolution that eliminates the need for increasing the number of discrete crystal orientations to account for new orientations created by twinning during deformation. The polycrystal is represented by an orientation distribution function using the Rodrigues parameterization. A total Lagrangian framework is used to model the evolution of microstructure. Numerical examples are used to show the application of the methodology for modeling deformation processes.

*PACS:* 61.72.Mm;61.72.-y;81.40.Ef

*Keywords:* Polycrystal plasticity; Texture; Twinning; Slip; Finite element analysis

---

---

<sup>1</sup> Corresponding author: Fax: +607-255-1222.  
Email: zabaras@cornell.edu  
URL: <http://mpdc.mae.cornell.edu/>

## 1 Introduction

There have been significant developments in the field of crystal plasticity modeling and evolution of microstructure. For deformation of FCC and BCC metals which deform predominantly by crystallographic slip there is already a well developed mathematical theory [1–5]. Plastic deformation of hexagonal closed packed crystalline (HCP) materials due to slip and twinning is less developed. HCP materials are characterized by highly anisotropic mechanical behavior. Twinning and slip have shown to be important deformation modes for these materials at low temperature. Hence, realistic modeling of HCP crystalline materials requires modeling of the deformation twinning in the constitutive equations.

The closed packed directions for crystallographic slip on HCP materials are  $\langle 11\bar{2}0 \rangle$  family of directions. Since these are perpendicular to the c-axis of the HCP crystals they lack the ability to cause deformation along that axis. Twinning is considered to be the mechanism that provides the inelastic deformation along the c-axis.

The problem of incorporating the twinning mechanism into crystal plasticity has been addressed in [6–10]. In these works, twinning is treated as pseudo-slip and it is assumed that there exist a critical resolved shear stress for twinning systems. Since twinning consists of a sudden change in crystal orientation, texture evolution due to twinning is different from that of slip. Various models have been used to model texture evolution due to twinning. One of the major difficulties in addressing the texturing due to twinning has been to account for the new crystal orientation generated by the twinning. In [7,11] a probabilistic approach is used to avoid the difficulties associated with increasing number of discrete crystal orientations. In these models, the orientations of grains are updated only if the twinned volume fraction has reached a certain value.

Theoretical investigations of texture development are typically based on discrete aggregate models. In these models, the polycrystal response is modeled through a representative volume of material with discrete aggregates. An alternative method for texture evolution is to use a continuous representation of orientation through the orientation distribution function (ODF) [6]. In this method, the distribution of crystal orientations is modeled over a three-dimensional orientation space. Finite element schemes for the ODF were proposed in [4–6,12,13]. These are based on a finite element representation of the ODF using piecewise polynomial interpolating functions. This approach avoids using discrete orientations and problems associated with increasing the number of elements to account for new orientations created by twinning during the process. However, it lacks the ability to capture grain boundary accommodation and interaction between grains.

Further, in contrast to existing works, based almost entirely on Euler angle spaces, the analysis of HCP polycrystals that follows is based on Rodrigues' space. Using this representation one can use the crystal symmetries to reduce the space to a geometrically simple region [6]. This will allow the texture evolution equations to be solved over a reduced region of the space called fundamental region. Moreover, due to symmetry of the space, textures have a particularly simple structure over Rodrigues' space. On this representation, a conservation equation for the ODF evolution for material deforming by combinations of multiple slip and twinning is introduced similar to [6] which takes into account sudden jumps in orientations as a consequence of twinning.

The orientation distribution function is updated in Rodrigues space by solving this conservation type equation using the finite element method. In addition to modelling texture evolution, this also provides the means to predict the response of HCP polycrystals. In [6], a constitutive model was employed for HCP polycrystals but no effort was made in modeling the material stress-strain response.

In this paper, a rate-independent constitutive model is used for predicting the response of HCP polycrystals due to slip and twinning. Grain boundary effects are incorporated in the simulation using the approach suggested in [7]. A new probabilistic criterion for arresting twinning is proposed which is capable of predicting different strain hardening stages reported in the literature. A total Lagrangian approach is used to model the texture evolution. The continuum representation of texture used in this paper, enables one to model the texture evolution independent of the choice of an aggregate and to avoid the difficulties associated with increasing the number of discrete crystal orientations due to twinning. The model is validated for tension, shear and compression modes.

The plan for the paper is as follows. In Section 2, the mathematical model for twinning is discussed and it is shown that twinning can be considered as a pseudo-slip. In Section 3, a continuum description of polycrystals is represented along the necessary equations for texture evolution. In Section 4 the constitutive model for polycrystals undergoing slip and twinning is represented. Section 5 discusses the reorientation of crystals. Section 6 presents some numerical applications of the methodology. Section 7 contains the discussion.

## 2 Twinning model

In modeling the twin as a pseudo-slip, the approach in [6] is adopted here. Consider a single crystal consisting of untwinned and twinned parts with volume fraction of the twinned part equal to  $\lambda$ . Let  $\mathbf{n}^{tw}$  be a unit normal vector to the twinning plane and  $\mathbf{b}^{tw}$  be the twinning plane direction (Fig. 1). Let  $\mathbf{x}$  be the original position of a lattice point and  $\mathbf{x}'$  be its twinned position. The displacement under twinning is proportional to  $\mathbf{x} \cdot \mathbf{n}^{tw}$  [6]:

$$\mathbf{x}' = \mathbf{x} + \gamma_0 \mathbf{b}^{tw} (\mathbf{x} \cdot \mathbf{n}^{tw})$$

$$= (I + \gamma_0(\mathbf{b}^{tw} \otimes \mathbf{n}^{tw}))\mathbf{x} = \mathbf{F}^{tw}\mathbf{x} \quad (1)$$

where  $\gamma_0$  is a constant of proportionality and  $\mathbf{F}^{tw}$ , the deformation gradient for the twinned part. The deformation gradient for the untwinned part is the identity tensor ( $\mathbf{F}^{ntw} = \mathbf{I}$ ). The average deformation gradient for the grain is calculated as follows:

$$\mathbf{F} = \lambda\mathbf{F}^{tw} + (1 - \lambda)\mathbf{F}^{ntw} = \mathbf{I} + \lambda\gamma_0\mathbf{b}^{tw} \otimes \mathbf{n}^{tw} \quad (2)$$

Since in this model twinning occurs continuously,  $\dot{\lambda}$  exists and is finite. Hence, the average macroscopic velocity gradient for the entire grain can be written as [6]:

$$\mathbf{L} = \dot{\mathbf{F}}\mathbf{F}^{-1} = \dot{\lambda}\gamma_0\mathbf{b}^{tw} \otimes \mathbf{n}^{tw} = \dot{\gamma}\mathbf{S}^{tw} \quad (3)$$

From this we see that twinning on a single twin system could be considered as a pseudo-slip with the shear rate  $\dot{\gamma}$  and Schmid tensor

$$\mathbf{S}^{tw} = \mathbf{b}^{tw} \otimes \mathbf{n}^{tw}.$$

### 3 Overview of representation of HCP polycrystals

To set forward the necessary background for later developments, a very brief description of microstructure associated with polycrystalline plasticity is provided. Consider a macroscopic material point and let it be associated with the underlying microstructure  $\mathcal{M}$ . Using the Taylor hypothesis, response of any crystal of the polycrystal is determined only by its orientation and does not depend on attributes of neighboring crystals. The rotation  $\mathbf{R}$  relates the crystal lattice frame,  $\hat{\mathbf{e}}_i$ , to a sample reference frame  $\mathbf{e}_i$  as  $\mathbf{e}_i = \mathbf{R}\hat{\mathbf{e}}_i$ . The orientation  $\mathbf{R}$  is not unique because of crystal symmetries. This non-uniqueness has traditionally been resolved by restricting the choice of orientation to a fundamental region.

The ODF (orientation distribution function), represented as  $\mathcal{A}(\mathbf{r})$ ,

is used to represent the crystal density over the fundamental region. In this paper, the representation of the ODF given by  $\mathcal{A}(\mathbf{r}, t)$  is Eulerian and  $\hat{\mathcal{A}}(\mathbf{s}, t)$  is Lagrangian ( $\mathcal{A}(\mathbf{r}, t) = \mathcal{A}(\hat{\mathbf{r}}(s, t), t) = \hat{\mathcal{A}}(\mathbf{s}, t)$ ). When texture development is modeled, a reorientation vector  $\hat{\mathbf{r}}(s, t)$  is computed that maps the location  $\mathbf{r}$  in the reoriented region (at time  $t$ ) to the corresponding location  $s$  in the reference fundamental region (at time  $t = 0$ ).

The evolution of ODF can be considered by the conservation equation which in the Lagrangian framework has the following format [14]

$$\int_{\Omega} \left( \hat{\mathcal{A}}(\mathbf{s}, t) J(\mathbf{s}, t) - \hat{\mathcal{A}}(\mathbf{s}, 0) \right) d\Omega = 0 \quad (4)$$

where  $J(\mathbf{s}, t)$  is the Jacobian determinant of the re-orientation of the crystals and  $\hat{\mathcal{A}}(\mathbf{s}, 0) = \mathcal{A}_0(\mathbf{s})$  is the ODF associated with the reference map and can be thought of as the initial texturing of the material. The Lagrangian version of the conservation equation is then defined as:

$$\hat{\mathcal{A}}(\mathbf{s}, t) J(\mathbf{s}, t) = \hat{\mathcal{A}}(\mathbf{s}, 0) = \mathcal{A}_0(\mathbf{s}) \quad (5)$$

The conventional Eulerian rate form of the conservation equation is obtained by considering the rate of Eq. (5) as

$$\begin{aligned} \frac{\partial \mathcal{A}(\mathbf{r}, t)}{\partial t} + \nabla \mathcal{A}(\mathbf{r}, t) \cdot \mathbf{v}(\mathbf{r}, t) \\ + \mathcal{A}(\mathbf{r}, t) \nabla \cdot \mathbf{v}(\mathbf{r}, t) = 0 \end{aligned} \quad (6)$$

where  $\mathbf{v}(\mathbf{r}, t)$  is the Eulerian re-orientation velocity. Such an Eulerian representation of the ODF is useful in cases where elastic effects are negligible. In a Lagrangian framework, the reorientation  $\hat{\mathbf{r}}$  has to be calculated from the reorientation velocity using the following relation:

$$\frac{d\hat{\mathbf{r}}}{dt} = \hat{\mathbf{v}}(\mathbf{r}, t) \quad (7)$$

The Jacobian determinant of the reorientation of the crystals can then be calculated as  $J(\mathbf{r}, t) = \det(\nabla(\hat{\mathbf{r}}))$ .

### 3.1 Representing twinning in the orientation space

Twinning can be modeled as the reflection of the orientation in the twinning plane. Let  $\mathbf{n}$  be the unit vector normal to the twinning plane. The mapping of the crystal through twinning can be represented as [15]:

$$\mathbf{x}' = \mathbf{x} - 2\mathbf{n}(\mathbf{n} \cdot \mathbf{x}) = (\mathbf{I} - 2\mathbf{n} \otimes \mathbf{n})\mathbf{x} = T_1\mathbf{x} \quad (8)$$

where  $T_1 = \mathbf{I} - 2\mathbf{n} \otimes \mathbf{n}$  and  $\mathbf{I}$  is the identity matrix. Since this mapping represents a reflection, one would end up with  $\det T_1 = -1$ . To represent this mapping with rotation, we need to have  $\det T = +1$ . We can achieve this through another reflection  $\det T_2 = -1$  that maps the lattice to itself. The resultant map would be  $T = T_2 T_1$ . Since all the crystallographic lattices are symmetric with respect to reflection around the origin, one can choose  $T_2 = -I$ . For the 3D case,  $\det T_2 = -1$  and one will end up with [15]

$$\begin{aligned} \mathbf{T}\mathbf{x} &= (-\mathbf{I})(-\mathbf{I} + 2\mathbf{n} \otimes \mathbf{n})\mathbf{x} \\ &= (\mathbf{I} - 2\mathbf{n} \otimes \mathbf{n})\mathbf{x} = T_1\mathbf{x} \end{aligned} \quad (9)$$

The resultant operator  $T$  can be seen as rotation of crystal axis about the twin plane normal through an angle of  $\pi$ . Under the quaternion parametrization of rotation space, this rotation can be represented by a quaternion:

$$T^q = \pm[0, \mathbf{n}] \quad (10)$$

The steps required for calculating the lattice reorientation in the fundamental region due to twinning is summarized as follows:

- (1) Convert parametrization of crystal lattice orientation in Rodrigues space ( $\mathbf{h}$ ) to the quaternion representation ( $\mathbf{h}^q$ ).
- (2) Perform the quaternion product  $\mathbf{q} = T^q \mathbf{h}^q$
- (3) Project  $\mathbf{q}$  to an equivalent rotation  $\mathbf{q}^F$  in the fundamental region based on crystal symmetries.
- (4) Convert  $\mathbf{q}^F$  to the Rodrigues parametrization,  $\mathbf{h}^{new}$ .

### 3.2 Conservation of the ODF considering slip and twinning

Twinning of the crystal lattice on a particular twin system uniquely maps the orientation to another location in the fundamental region. Thus, twinning results in loss of volume fraction of a particular orientation and accumulation of the orientation at another location in the orientation space. These can be regarded as source and sink terms in the conservation equation (Eq. 4). Since the material volume must be conserved, material leaving from a source must show up at a sink.

At an orientation  $A(\mathbf{r}, t)$ , the source ( $\phi$ ) at an instant  $t$  contains two terms arising from the loss of volume fraction of that orientation due to twinning and the gain of orientation from its twin images at positions  $\mathbf{r}^k$  in the orientation space. This is shown schematically in Fig. 2. Thus  $\phi(A, \mathbf{r}, t)$  is given as [6],

$$\begin{aligned} \phi(A, \mathbf{r}, t) = & \sum_{k \in \alpha_{tw}} A(\mathbf{r}^k, t) \dot{\lambda}^k(\mathbf{r}^k) \\ & - A(\mathbf{r}, t) \sum_{k \in \alpha_{tw}} \dot{\lambda}^k(\mathbf{r}) \end{aligned} \quad (11)$$

Here,  $\alpha_{tw}$  is the set of images of the current crystal orientation with respect to the twin planes of the twin systems and  $\dot{\lambda}^k$  refers to the rate of change in volume fraction of the orientation at time  $t$  due to twinning in the twin system given by  $k$ . Thus, the presence of the conservation term modifies the evolution of the ODF in the form,

$$\begin{aligned} \int_{\Omega} J(\mathbf{s}, t)(\hat{A}(\mathbf{s}, t) - \Phi(\mathbf{s}, t))d\Omega \\ = \int_{\Omega} \hat{A}(\mathbf{s}, 0)d\Omega \end{aligned} \quad (12)$$

where  $\Omega$  is the reference fundamental region and

$$\Phi(\mathbf{s}, t) = \int_0^t \phi(\mathbf{s}, t)dt \quad (13)$$

The total volume fraction of twinned crystals can be calculated by only considering the untwinned portion ( $\tilde{A}$ ) of the ODF as,

$$\begin{aligned} \int_{\Omega} J(\mathbf{s}, t)(\tilde{A}(\mathbf{s}, t) - \tilde{\Phi}(\mathbf{s}, t))d\Omega \\ = \int_{\Omega} \hat{A}(\mathbf{s}, 0)d\Omega \end{aligned} \quad (14)$$

Here, the source term due to the presence of twinning ( $\tilde{\Phi}$ ) is given as [6],

$$\tilde{\Phi}(\mathbf{s}, t) = \int_0^t \tilde{\phi}(\mathbf{s}, t)dt \quad (15)$$

and

$$\tilde{\phi}(\mathbf{s}, t) = -\tilde{A}(\mathbf{s}, t) \sum_{k \in \alpha_{tw}} \dot{\lambda}^k(\mathbf{s}) \quad (16)$$

Only the volume fraction that is lost from each orientation is calculated. The other term in  $\phi(\mathbf{s}, t)$  that corresponds to the orientations coming from the other twin images is not used. Since we concentrate only on the volume fraction of crystals that is lost due to twinning, the equation for ( $\tilde{A}$ ) no longer follows ODF conservation. The volume fraction of twins is given by  $\tilde{A}(\mathbf{s}, t)$  as,

$$f = 1 - \int_{\Omega} \tilde{A}(\mathbf{s}, t) d\Omega \quad (17)$$

The ODF, in the present work, is approximated with finite element polynomial functions defined over an explicit discretization of the orientation space based on Rodrigues parametrization. The parametrization of  $\mathbf{R}$  is derived from the natural invariants of  $\mathbf{R}$ : the axis of rotation  $\mathbf{n}$  and the angle of rotation  $\zeta$ . The angle-axis parametrization ( $\mathbf{r}$ ) is obtained by scaling the axis  $\mathbf{n}$  by a function of the angle  $\zeta$  as  $\mathbf{r} = \mathbf{n} \tan\left(\frac{\zeta}{2}\right)$ . The orientation  $\mathbf{R}$  is related to the parametrization  $\mathbf{r}$  as

$$\begin{aligned} \mathbf{R} &= \frac{1 - \mathbf{r} \cdot \mathbf{r}}{1 + \mathbf{r} \cdot \mathbf{r}} (\mathbf{I}) \\ &+ \frac{2}{1 + \mathbf{r} \cdot \mathbf{r}} (\mathbf{r} \otimes \mathbf{r} + \mathbf{I} \times \mathbf{r}) \end{aligned} \quad (18)$$

The polycrystal average of an orientation dependent property,  $\Upsilon(\mathbf{r}, t)$ , is determined as follows

$$\begin{aligned} \langle \Upsilon \rangle &= \int_{\Omega_t} \Upsilon(\mathbf{r}, t) \mathcal{A}(\mathbf{r}, t) d\Omega_t \\ &= \int_{\Omega} \Upsilon(\hat{\mathbf{r}}(\mathbf{s}, t), t) (\mathcal{A}_0(\mathbf{s}) \\ &+ \Phi(\mathbf{s}, t) J(\mathbf{s}, t)) d\Omega \end{aligned} \quad (19)$$

where  $d\Omega_t$  is defined as the volume element on the current fundamental region. One can conclude that if the re-orientation and initial texture are known the average property for the polycrystal can be calculated. Hence, there is no need to compute the current ODF,  $\mathcal{A}(\mathbf{r}, t)$ .

#### 4 Constitutive sub-problem for HCP crystals deforming through slip and twinning

During deformation process of a HCP polycrystal, the deformation is manifested in the crystal in the form of crystallographic slip, twinning and lattice re-orientation of crystals. Re-orientation of the crystals occurs in an ordered manner such that a preferential orientation or texture develops. Consider a point on the reference fundamental region corresponding to a particular crystal orientation. In an appropriate kinematic framework for large deformation inelastic analysis, the total deformation gradient is decomposed into plastic and elastic parts as follows (Fig. 3)

$$\mathbf{F}_{n+1} = \mathbf{F}^e \mathbf{F}^p \quad (20)$$

where  $\mathbf{F}^e$  is the elastic deformation gradient and  $\mathbf{F}^p$ , the plastic deformation gradient, with  $\det \mathbf{F}^p = 1$ . This decomposition of the deformation gradient results in the following

$$\mathbf{F}^e = \mathbf{F}_{n+1} (\mathbf{F}^p)^{-1} \quad (21)$$

In the following scheme, all vector and tensorial quantities are expressed in the reference sample frame, i.e., the initial (macro-scale) configuration. Furthermore, crystal specific properties like the stiffness and compliance have to be transformed to the sample reference frame using the crystal orientation  $\mathbf{r}$ . At time  $t = t_{n+1}$ , the following steps are followed to update the texture and obtain the necessary quantities at a material point in the sample. The data that is known at time  $t = t_{n+1}$  includes  $\{\mathbf{F}_n, \mathbf{F}_{n+1}\}$ , the deformation gradients at time  $t = t_n$  and  $t_{n+1}$ , the Cauchy stress  $\mathbf{T}_n$  and the ODF  $A(\mathbf{r}, t_n)$  at time  $t_n$ . The task of the constitutive sub-problem is to identify the elastic-plastic decomposition of the deformation gradient and the Cauchy stress at time  $t_{n+1}$ . Further, this information is used to calculate reorientation of the crystals which is in turn used to update the ODF.

In the constitutive equations to be defined below, the Green elastic strain measure is defined on the relaxed configuration (plastically deformed, unstressed configuration)  $\bar{\mathcal{B}}$ . It is represented as  $\bar{\mathbf{E}}^e = \frac{1}{2}(\mathbf{F}^{eT}\mathbf{F}^e - \mathbf{I})$ . The conjugate stress measure is then defined as  $\bar{\mathbf{T}} = \det\mathbf{F}^e(\mathbf{F}^e)^{-1}\mathbf{T}(\mathbf{F}^e)^{-T}$  where  $\mathbf{T}$  is the Cauchy stress for the crystal in the sample reference frame. In the following analysis, crystal specific properties like the stiffness and compliance are transformed to the sample reference frame for each crystal using the position  $\mathbf{r}$  in the orientation space. The trial elastic strain ( $\bar{\mathbf{E}}_{trial}^e$ ) is first calculated as:

$$\begin{aligned}\mathbf{F}_{trial}^e &= \mathbf{F}(\mathbf{F}_n^p)^{-1} \\ \bar{\mathbf{E}}_{trial}^e &= \frac{1}{2}((\mathbf{F}_{trial}^e)^T\mathbf{F}_{trial}^e - \mathbf{I})\end{aligned}\tag{22}$$

This is followed by a calculation of a trial stress  $\bar{\mathbf{T}}_{trial}$  and trial resolved shear stress  $\tau_{trial}^\alpha$  on each slip and twin system:

$$\begin{aligned}\bar{\mathbf{T}}_{trial} &= \mathbf{L}^e[\bar{\mathbf{E}}_{trial}^e] \\ \tau_{trial}^\alpha &= \bar{\mathbf{T}}_{trial} \cdot \mathbf{S}_0^\alpha\end{aligned}\tag{23}$$

Here  $\mathbf{S}_0^\alpha = \mathbf{m}^\alpha \otimes \mathbf{n}^\alpha$  is the Schmid tensor and  $\dot{\gamma}^\alpha$  is the plastic shearing rate on the  $\alpha^{th}$  slip or twin system.  $\mathbf{m}^\alpha$  and  $\mathbf{n}^\alpha$  are the slip or twin direction and plane normal, respectively. There is a critical resolved shear stress above which slip and twin systems are activated. Such a set  $\mathcal{PA}$  of potentially active slip and twin systems are identified initially based on the trial resolved stress as the systems with  $|\tau_{trial}^\alpha| - s^\alpha(t) > 0$ .

The evolution of plastic deformation gradient can be written as

$$\dot{\mathbf{F}}^p = \mathbf{L}^p\mathbf{F}^p\tag{24}$$

The flow rule should be modified to take into account the grain boundary accommodation effect. In [7], the use of an extra isotropic term is suggested for this purpose. The shearing rates on the slip and twin systems,  $\dot{\gamma}^\alpha$  is found using the following flow rule,

$$\mathbf{L}^p = (1 - \xi) \sum_{\alpha} \dot{\gamma}^\alpha \text{sign}(\tau^\alpha) \mathbf{S}_0^\alpha + \xi \mathbf{M} \quad (25)$$

$$\mathbf{M} = \dot{\epsilon}_0 \left( \frac{\bar{\sigma} - s_{th}}{s} \right)^{\frac{1}{m}} \left( \frac{3\mathbf{T}'}{2\bar{\sigma}} \right) \quad (26)$$

$$\bar{\sigma} = \sqrt{\frac{3}{2} \mathbf{T}' \cdot \mathbf{T}'} \quad (27)$$

where  $\dot{\epsilon}_0$  is a constant,  $\xi$  is nonzero only if  $\bar{\sigma} > s_{th}$  and  $s$  is an internal variable with a threshold value  $s_{th}$ . As suggested in [7], the localized non-crystallographic effects around grain boundaries can be approximated by a grain boundary layer with a very small volume fraction ( $\xi \ll 1$ ). The layer is assumed to follow a simple isotropic flow rule. Hence, the isotropic term is added to the flow rule to account for grain boundary effects. Since the assumption of fully bounded grains leads to unrealistically high stress this term helps in bounding the stress level.

Using an Euler-backward time integration procedure, one can write,

$$\mathbf{F}_{n+1}^p = (\mathbf{I} + \Delta t \mathbf{L}^p) \mathbf{F}_n^p \quad (28)$$

Substituting Eq. (28) in Eq. (21) results in

$$\mathbf{F}_{n+1}^p = \mathbf{F}_{trial}^e (\mathbf{I} - (1 - \xi) \Delta t \times \sum_{\alpha} \dot{\gamma}^\alpha \text{sign}(\tau^\alpha) \mathbf{S}_0^\alpha - \xi \mathbf{M} \Delta t) \quad (29)$$

During plastic flow the active systems are assumed to follow the consistency condition:  $|\boldsymbol{\tau}^\alpha| = s^\alpha$  and a simple non hardening assumption is used for the slip and twin resistances ( $\dot{s}(i) = 0$ ). The bar stress (the conjugate to the green elastic strain; the second Piola-Kirchhoff stress) is then given by,

$$\begin{aligned} \bar{\mathbf{T}} &= \bar{\mathbf{T}}_{trial} - (1 - \xi) \frac{\Delta t}{2} \sum_{\beta} \text{sign}(\boldsymbol{\tau}_{trial}^\beta) \dot{\gamma}^\beta \mathbf{L}^e[\mathbf{B}^\beta] \\ &\quad - \xi \frac{\Delta t}{2} \mathbf{L}^e(\mathbf{F}_{trial}^e{}^T \mathbf{F}_{trial}^e \mathbf{M} + (\mathbf{M})^T \mathbf{F}_{trial}^e{}^T \mathbf{F}_{trial}^e) \end{aligned} \quad (30)$$

The updated shearing rates  $\dot{\gamma}^\beta$  are obtained by solving the following equation:

$$\begin{aligned} |\boldsymbol{\tau}^\alpha| &= |\boldsymbol{\tau}_{trial}^\alpha| - (1 - \xi) \frac{\Delta t}{2} \times \\ &\sum_{\beta} \text{sign}(\boldsymbol{\tau}_{trial}^\alpha) \text{sign}(\boldsymbol{\tau}_{trial}^\beta) \dot{\gamma}^\beta \mathbf{L}^e[\mathbf{B}^\beta] \cdot \mathbf{S}_0^\alpha \\ &\quad - \xi \frac{\Delta t}{2} \text{sign}(\boldsymbol{\tau}_{trial}^\alpha) \mathbf{L}^e(\mathbf{F}_{trial}^e{}^T \mathbf{F}_{trial}^e \mathbf{M} \\ &\quad + (\mathbf{M})^T \mathbf{F}_{trial}^e{}^T \mathbf{F}_{trial}^e) \cdot \mathbf{S}_0^\alpha \end{aligned} \quad (31)$$

where,  $\alpha \in \mathcal{PA}$  and,

$$\mathbf{B}^\beta = [(\mathbf{S}_0^\beta)^T (\mathbf{F}_{trial}^e)^T \mathbf{F}_{trial}^e + (\mathbf{F}_{trial}^e)^T \mathbf{F}_{trial}^e \mathbf{S}_0^\beta] \quad (32)$$

The system of equations for  $x^\beta = \dot{\gamma}^\beta \geq 0$  takes the form:

$$\sum_{\beta \in \mathcal{PA}} A^{\alpha\beta} x^\beta = b^\alpha \quad (33)$$

where,

$$A^{\alpha\beta} = \frac{\Delta t}{2} \text{sign}(\boldsymbol{\tau}_{trial}^\alpha) \text{sign}(\boldsymbol{\tau}_{trial}^\beta) \mathbf{L}^e[\mathbf{B}^\beta] \cdot \mathbf{S}_0^\alpha$$

(34)

$$\begin{aligned}
b^\alpha &= |\boldsymbol{\tau}_{trial}^\alpha| - s^\alpha - \xi \frac{\Delta t}{2} \text{sign}(\boldsymbol{\tau}_{trial}^\alpha) \\
&\times \mathbf{L}^e (\mathbf{F}_{trial}^e)^T \mathbf{F}_{trial}^e \mathbf{M} \\
&+ (\mathbf{M})^T \mathbf{F}_{trial}^e (\mathbf{F}_{trial}^e)^T \cdot \mathbf{S}_0^\alpha
\end{aligned} \tag{35}$$

If for any slip system  $\dot{\gamma}^\beta \leq 0$ , then this slip system is removed from the set of potentially active systems. The system of Eqs. (33) is solved until for all slip systems  $\dot{\gamma}^\beta > 0$ .

The plastic part of the deformation gradient and the Cauchy stress are computed as follows,

$$\begin{aligned}
\mathbf{F}^p &= (\mathbf{I} + \Delta t \mathbf{L}^p) \mathbf{F}_n^p \\
\mathbf{T} &= F^e [\det(\mathbf{F}^e)]^{-1} \bar{\mathbf{T}} (F^e)^T
\end{aligned} \tag{36}$$

The change in the volume fraction of twin systems used in Eq. (3) for updating the average macroscopic velocity gradient is now given as,

$$\dot{\lambda}^\alpha(t) = \frac{\dot{\gamma}^\alpha}{\gamma_0} \tag{37}$$

## 5 Reorientation of crystals

The reorientation velocity is given as follows:

$$\mathbf{v} = \frac{\partial \mathbf{r}}{\partial t} = \frac{1}{2} (\boldsymbol{\omega} + (\boldsymbol{\omega} \cdot \mathbf{r}) \mathbf{r} + \boldsymbol{\omega} \times \mathbf{r}) \tag{38}$$

where  $\mathbf{r}$  is the orientation (Rodrigues' parametrization) and  $\boldsymbol{\omega}$  represents the spin vector defined as  $\boldsymbol{\omega} = \text{vect}(\dot{\mathbf{R}}^e \mathbf{R}^{eT}) = \text{vect}(\boldsymbol{\Omega})$  where  $\mathbf{R}^e$  is evaluated through the polar decomposition of the elastic deformation gradient  $\mathbf{F}^e$  as  $\mathbf{F}^e = \mathbf{R}^e \mathbf{U}^e$ . Considering the Euler-backward time integration of  $\dot{\mathbf{R}}^e \mathbf{R}^{eT} = \boldsymbol{\Omega}$ , where  $\boldsymbol{\Omega}$  is the spin tensor, leads to the following:

$$\mathbf{R}_{n+1}^e = \exp(\Delta t \boldsymbol{\Omega}_{n+1}) \mathbf{R}_n^e \quad (39)$$

and

$$\boldsymbol{\Omega}_{n+1} = \frac{1}{\Delta t} \ln \{ \mathbf{R}_{n+1}^e \mathbf{R}_n^{eT} \} \quad (40)$$

From the elastic deformation gradients,  $\mathbf{R}_{n+1}^e$  and  $\mathbf{R}_n^e$  are evaluated and one can evaluate the spin tensor  $\boldsymbol{\Omega}_{n+1}$  using Eq. (40) and then the re-orientation velocity from Eq. (38). Further, post-processing involves computing the average Cauchy stress from

$$\langle \mathbf{T} \rangle = \int_{\Omega_t} \mathbf{T}(\mathbf{r}, t) \mathcal{A}(\mathbf{r}, t) d\Omega_t \quad (41)$$

### 5.1 Arresting of twin systems

Experimental results show that the volume fraction of twins for HCP materials saturates at a level significantly smaller than unity [16]. This shows that after twinning starts some restriction must be imposed on propagation of twins.

A number of different mechanisms have been proposed to determine where the deformation twinning activity should stop [6,16]. In [6], it is assumed that twins are not likely to form if they are going to intersect existing twins. A random function was used to relate the probability of intersection of twins to their volume fraction. Then this random function is used to stop the twinning activity. The random function was constructed from geometric

arguments in which a hypothetical grain is considered as an average of real grains.

As suggested in [17], only a small portion of grains show cross twinning in comparison to the total number of twins. Hence, for arresting the twin systems the following method is used. For almost all twin systems, the twinning is stopped after the saturation volume fraction is reached. However, based on a probabilistic criterion given below, some of these twin systems may get activated. This method is used to activate the primary systems that undergo twinning and deactivate the rest due to obstacles to twinning. The small probability of cross twinning is also taken into consideration by allowing the twinning to happen after the twinning volume fraction passes the saturation volume fraction and satisfies the inequality criterion described below. The algorithm used for arresting twinning is summarized below:

$$\begin{aligned}
 f < f_{sat} & \text{ twinning is allowed} \\
 f > f_{sat} & \text{ twinning is allowed only if } f > P_f
 \end{aligned}$$

where  $P_f$  is a random variable. In this paper,  $P_f$  is assumed to have a uniform random distribution between 0.3 and 1.0 [7] and  $f_{sat}$  is assumed to be 0.2 as suggested in [6].

## 6 Numerical results

### 6.1 Example 1: Validation of texture evolution for Titanium

In this example texture evolution is examined for Titanium which has a HCP structure. A plane strain compression mode is assumed with a true strain rate equal to unity. The active slip and twinning systems are shown in Table 1. The values used for the elastic moduli are the following [18]:

$$C_{11} = 256.6 \text{ GPa}, C_{12} = 0.36 \text{ GPa}, C_{13} = 69.7 \text{ GPa}, C_{33} =$$

325.13  $GPa$ ,  $C_{55} = 46.71 GPa$ .

No grain boundary effect is considered for this example. The following material parameters for slip and twinning systems are used for constitutive model:

$s_{basal} = 8.0 MPa$ ,  $s_{prismatic} = 1.0 MPa$ ,  $s_{pyramidal} = 10.0 MPa$  and  $s_{twin} = 1.25 MPa$ .

The initial texturing of the material is assumed to be random. The orientation distribution function is represented in Rodrigues space in Fig. 4. The reference fundamental region is obtained from this space after applying the necessary HCP crystal symmetries. It is discretized into 111 tetrahedral elements. The total Lagrangian ODF corresponding to an effective strain of  $\varepsilon = 0.5$  is shown in Fig. 5. It is in a very good agreement with the results of [6] shown in the same figure.

## 6.2 Example 2: Validation of constitutive model and texture evolution for Titanium

For validating the constitutive model  $\alpha$ -titanium is used in this example. The result of stress-strain curve and final texture is compared with the experimental result reported in [19]. No grain boundary effect is considered for this example and the same slip and twinning systems as Example 1 are used with the following material parameters taken from [19]

$s_{basal} = 150 MPa$ ,  $s_{prismatic} = 30 MPa$ ,  $s_{pyramidal} = 120 MPa$ ,  $s_{twin} = 125 MPa$ .

It should be emphasized here that the differences between the material parameters used in [6,19] is due to the fact that in [6] there was no attempt to match the stress-strain response with

experimental results.

The initial texturing of the material is assumed to be random. The texture prediction for simple shear mode shown in Fig. 6 is in a good agreement with experimental results reported by Wu et al. [19]. The predicted result captures the strong textures in  $\{0001\}$  and  $\{10\bar{1}0\}$  pole figures. Although the work in [19] failed to completely capture the strong features seen in  $\{0001\}$  pole figure obtained from experiment, the present work was able to show a good agreement with the experimental result.

Finally, the predicted stress-strain response for the simple shear mode is compared with experimental data in Fig. 7. The experimental data and numerical result reported in [19] are in good agreement with the computed result in this work. It should be emphasized that in [19] a strain hardening model is used. The present work is thus able to capture well the strain hardening effect.

### *6.3 Example 3: Validation of constitutive model and texture evolution for magnesium alloy AZ31B*

To examine the constitutive model and the algorithm for texture evolution, magnesium alloy AZ31B (96.486% *Mg*, 2.798% *Al*, 0.715% *Zn*, *Balance*, *Mn*, *Fe*) is studied. The experimental results taken from [7] are obtained from a hot-extruded rod of alloy AZ31B subjected to tension and simple compression tests. The initial texture of the specimen is shown through  $\{0001\}$  and  $\{10\bar{1}0\}$  pole figures in Fig. 8. The material is subjected to a simple tension test with a constant true strain rate  $2 \times 10^{-4} s^{-1}$ . The following values are used for the elastic moduli [20]:

$$C_{11} = 58 \text{ GPa}, C_{12} = 25 \text{ GPa}, C_{13} = 20.8 \text{ GPa}, \\ C_{33} = 61.2 \text{ GPa}, C_{55} = 16.6 \text{ GPa}.$$

The operative slip and twinning systems are assumed to be basal  $(0001) \langle 11\bar{2}0 \rangle$ , prismatic  $10\bar{1}0 \langle 11\bar{2}0 \rangle$ , pyramidal  $10\bar{1}1 \langle 11\bar{2}0 \rangle$  slip systems and pyramidal  $10\bar{1}2 \langle \bar{1}011 \rangle$  twinning systems. These are shown in Table 1. The material parameters used for constitutive model are:

$$s_{basal} = 0.55 \text{ MPa}, s_{prismatic} = 105 \text{ MPa}, s_{pyramidal} = 105 \text{ MPa}, \\ s_{twin} = 18 \text{ MPa}.$$

for slip and twinning systems and

$$s_{th} = 170 \text{ MPa}, s = 220 \text{ MPa}, \dot{\varepsilon}_0 = 0.001 \text{ s}^{-1}, m = 0.07, \\ \xi = 0.05$$

for grain boundary accommodation [7].

The calculated  $\{0001\}$  and  $\{10\bar{1}0\}$  pole figures after 15% strain in simple tension are shown in Figure 9. Comparison between the final computed texture from the current study and the experimental data from [8] shows a good agreement. We believe that the failure of the computed crystallographic texture to show a perfect symmetric pattern in the  $\{10\bar{1}0\}$  polefigure is due to the fact that the current model considers the texture as a continuous distribution and spatial configuration of crystals is neglected. Whereas, in the experiment reported by Staroselsky and Anand [8] both the initial and final textures correspond to a specific spatial configuration of crystals.

The stress-strain curve is also compared in Fig. 10 with the results given in [7]. In [7], the polycrystal is modeled as a discrete set of orientations, whereas in this work, ODF representation of the polycrystal is used to avoid the dependency of the final result on the initial selection of the spatial configuration of the orientations. This work provides a general approach by representing all the structures that have the same orientation distribution. Although in both cases the initial pole figures look alike, the analysis in [7] is based on a specific selection and ordering of crystal orientations in the model. They argue that they select the initial

orientation of their discrete crystals such that they obtain the desired pole figures for the initial texture. In contrast, in the current method all textures with the desired pole figures are considered through the orientation distribution function. If a discrete representation of texture is used, one needs to split the finite elements to take into consideration the newly generated orientations due to twinning. In this work, however, application of a continuous representation of texture eliminates this problem.

The predictive capabilities of the model were also tested for the simple compression mode. The stress-strain curve is compared in Fig. 11. The computed result for texture evolution is given in Figure 12 and shows good agreement with the experiment data reported by Staroselsky and Anand [7].

Comparing Figs. 10 and 11, we note that the already reported [7] asymmetric behavior of tension and compression modes is apparent. This behavior can be explained by the evolution of the texture. The compressive mode of deformation and the initial texture makes the twinning and basal slipping to be more active. During the texture evolution the crystals align their  $c$  axis along the compression direction which makes the resolved shear stress on the basal plane to be very small and the pyramidal slip systems become active [7].

Again, the experimentally measured and numerically modeled response show a good agreement. The reader should notice that the model used by Staroselsky and Anand [7] considers the actual spatial configuration of the crystals and as they point out in their paper due to the non-hardening model used, the observed strain hardening is related to the evolution of the microstructure. Considering the fact that the current model neglects the exact spatial configuration of microstructure and uses a 1-st order representation, the stress-strain result shows an acceptable agreement with that of experiment. Notice that although a non-hardening model is used this work is able to capture the hardening part of the stress-strain curve by restricting the twinning after the satura-

tion limit is met. The strain hardening curve is also shown in Fig. 13. The same trend for strain hardening in simple compression mode is reported in [19]. It should be noticed that the  $f_{sat}$  and probability function  $P_f$  discussed earlier are responsible for the different stages seen in the figure.

Looking at Eq. (30) and neglecting the grain boundary effect for now (assuming  $\xi = 0$ ) makes this more clear. It is obvious that the role of the second term on the right hand side is to reduce the amount of stress. This reduction is caused proportional to the amount of plastic strain.

When volume fraction of the twinned part is less than  $f_{sat}$  all systems are allowed to contribute to the flow rule which causes stage A in which strain hardening is decreasing. After reaching  $f_{sat}$  the corresponding twin systems are taken out of the active systems which makes it harder for the plastic strain to develop, hence mimicking stage B which has an increasing strain-hardening rate. After the volume fraction of the twinned part passes the lower range of the  $P_f$  function, there will be a probability of including the twin systems in the active systems. This in turn initiates stage C which is characterized by a decreasing strain hardening rate.

From this example it is apparent that the method discussed in this work is able to reproduce the stress-strain relation and texture evolution of magnesium alloy AZ31B.

## 7 Conclusions

In this paper, a continuum approach for representing HCP polycrystals undergoing both slip and twinning is presented using a Lagrangian framework. The proposed methodology is applied to Titanium and Magnesium alloy AZ31B and the computed texture and stress-strain response have shown to be in good agreement with experiments and results from other numerical approaches.

The need for splitting existent elements to allow for newly generated orientations is eliminated by using a continuous method in the space of ODFs. This continuous method is general and can be used with any single crystal constitutive model. In addition, the probabilistic approach presented here is able to match experimental results using only a few parameters. In fact, the current non-hardening model is able to capture the macro- and micro-behavior of polycrystals without a need to search for hardening parameters. The proposed methodology is based on reported physical phenomena of twinning like saturation of twinning and existence of different stages in the strain-hardening regime.

The continuum representation of texture used in this paper represents the volume fraction of crystallographic orientations but it neglects the size, topology and shape of the grains. The authors recognize the fact that considering the spatial configuration of crystals leads to models that have greater flexibility in matching experimental data. The present model, however, is a great tool for fast exploration of the process/structure/property space since it was shown to reasonably represent the microstructure evolution without significant computational cost. In addition, the continuous representation of texture provides a natural framework for designing of texture-dependent properties using a mathematically rigorous continuum sensitivity method (CSM) [4,21]. When a viable texture distribution is obtained for desired material properties, a more accurate model can be used subsequently to investigate the effect of the spatial distribution of the microstructure. Work is on progress in applying this model to multiscale design applications.

## 8 Acknowledgements

The work presented here was funded by the Mechanical Behavior of Materials program (Dr. D. Stepp, program manager) of the Army Research Office and by the Materials Design and Surface

Engineering program of the NSF (award CMMI-0757824). Computing resources were provided in part by the Cornell Center for Advanced Computing.

## References

- [1] K.K. Mathur and P.R. Dawson, On modeling the development of crystallographic texture in bulk forming processes, *Int. J. Plast.* 5 (1989) 67-94.
- [2] A. Beaudoin, K.K. Mathur, P.R. Dawson and G.C. Johnson, Three dimensional deformation process simulation with explicit use of polycrystalline plasticity models, *Int. J. Plast.* 9 (1993) 833-860.
- [3] C.A. Bronkhorst, S.R. Kalidindi and L. Anand, Evolution of crystallographic texture during the deformation of FCC metals, in: T.C. Lowe et al., eds., *Modeling the deformation of crystalline solids (The minerals, metals and materials society, Warrendale)*, 1991.
- [4] S. Ganapathysubramanian, N. Zabaras, Design across length scales: A reduced-order model of polycrystal plasticity for the control of microstructure-sensitive material properties, *Comput Meth Appl Mech Engng.* 193 (2004) 5017-5034.
- [5] S. Ganapathysubramanian, N. Zabaras, Modeling the thermoelastic-viscoplastic response of polycrystals using a continuum representation over the orientation space, *Int J Plasticity* 21 (2005) 119-144.
- [6] S. Myagchilov, P.R. Dawson, Evolution of texture in aggregates of crystals exhibiting both slip and twinning, *Modell Simul. Mater. Sci. Eng.* 7 (1999) 975-1003.
- [7] A. Staroselsky, L. Anand, A constitutive model for hcp materials deforming by slip and twinning: application to magnesium alloy AZ31B, *Int. J. Plasticity* 19 (2003) 1843-1864.
- [8] A. Staroselsky, L. Anand, Inelastic deformation of polycrystalline face centered cubic materials by slip and twinning, *J Mech. Physics. Solids* 46 (1998) 671-696.
- [9] K.R. Kalidindi, Incorporation of deformation twinning in crystal plasticity models, *J Mech. Physics. Solids* 46 (1998) 267-271.
- [10] C. Tome, R.A. Lebenson, U.F. Kocks, A model for texture development dominated by deformation twinning: Application to zirconium alloys, *Acta Metall. Mater.* 39 (1991) 2667-2680.

- [11] P. Van Houtte, Simulation of the rolling and shear texture of brass by the Taylor theory adapted for mechanical twinning, *Acta Metall.* 26 (1978) 591-604.
- [12] A. Kumar, P.R. Dawson, Modeling crystallographic texture evolution with finite elements over neo-Eulerian orientation spaces, *Comput Meth Appl Mech Engng.* 153 (1998) 259-302.
- [13] S. Ganapathysubramanian, Design of deformation processes: Extending phenomenological and polycrystalline plasticity models towards the control of microstructure-sensitive properties, 2004; Ph.D. Thesis, Sibley School of Mechanical and Aerospace Engineering, Cornell University.
- [14] A. Clement, Prediction of deformation texture using a physical principle of conservation, *Mater. Sci. Engrg.* 55 (1982) 203-210.
- [15] S. Myagchilov, ODF evolution modeling for polycrystals experiencing multiple slip and twinning with finite elements over orientation space; Ph.D. thesis; Cornell Univeristy; 1998.
- [16] M. Philippe, M. Serghat, Modelling of texture evolution for materials of hexagonal symmetry-ii. application to zirconium and titanium, P. Van Houtte, C. Esling. *Acta Metall. Mater.* 43 (1995) 1619-1630.
- [17] S. Asgari, E. El Danaf, S.R. Kalidindi, R. Doherty, Strain hardening regimes and microstructural evolution during large strain compression of low stacking fault energy fcc alloys that form deformation twins, *Metall. Mater. Trans. A.* 28 (1997) 1781-1795.
- [18] W.F. Hosford, *The mechanics of crystals and textured polycrystals*, Oxford University Press, New York; 1993.
- [19] X. Wu, S.R. Kalidindi, C. Necker and A.A. Salem, Prediction of crystallographic texture evolution and anisotropic stress-strain curves during large plastic strains in high purity  $\alpha$ -titanium using a Taylor-type crystal plasticity model, *Acta Materialia.* 55 (2007) 423-432.
- [20] G. Simmons, H. Wang, *Single crystal elastic constants and calculated aggregate properties*, The M.I.T. Press, Cambridge; 1971.
- [21] S. Acharjee, N. Zabaras, The continuum sensitivity method for the computational design of three-dimensional deformation processes. *Comput Meth Appl Mech Engng.* 195 (2006) 6822-6842.

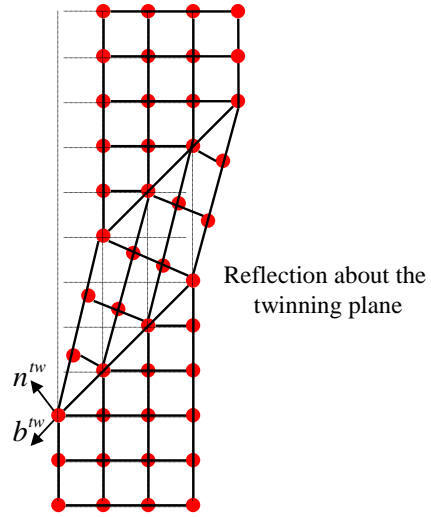


Fig. 1. The lattice in the twinned region has a special orientation in relation to the untwinned crystal, defined by a reflection across the twinning plane.

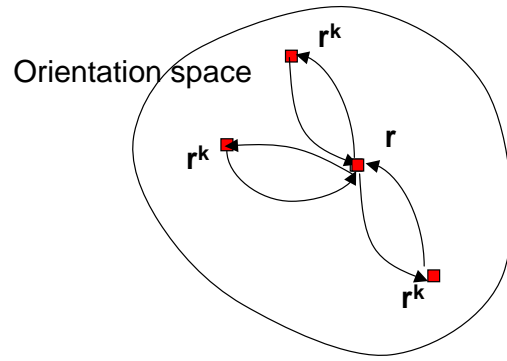


Fig. 2. Images of  $\mathbf{r}$  in the orientation space with respect to twin system  $k$ . The orientation  $\mathbf{r}$  acts as a source to the images  $\mathbf{r}^k$  while it gains volume fraction when it acts as a sink to the volume fraction lost by  $\mathbf{r}^k$ .

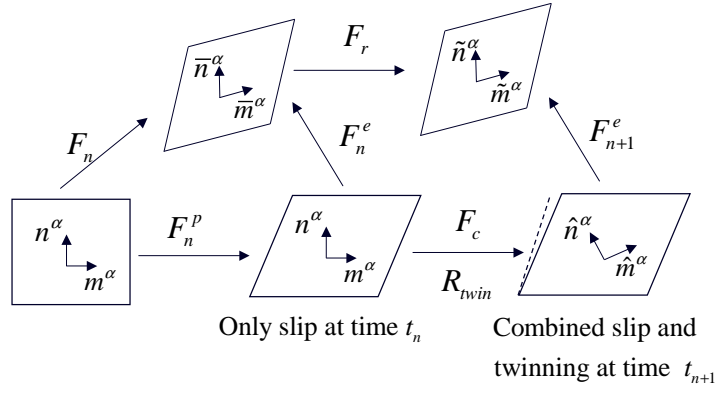


Fig. 3. Evolution of various material configurations for a single crystal as needed in the integration of the constitutive model. Here  $\mathbf{m}^\alpha$  denotes the slip direction and  $\mathbf{n}^\alpha$  denotes the slip normal, which together define the slip systems.  $\mathbf{F}_r$  is the relative deformation gradient. The mechanism at time  $t_n$  is slip alone. At time  $t_{n+1}$ , twin systems are activated which causes additional lattice reorientation ( $R_{twin}$ ) and a pseudo-slip.

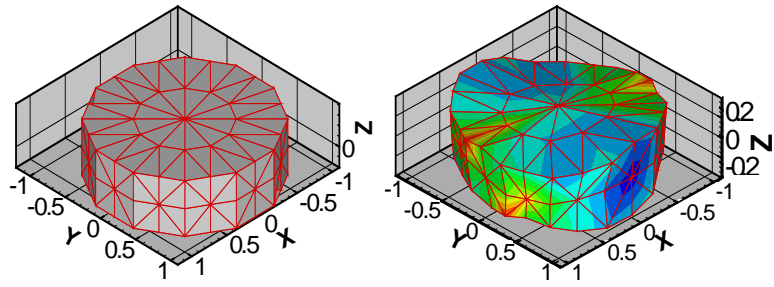


Fig. 4. (left) - Initial random texture shown in Rodrigues fundamental space for HCP symmetries; (right) - Computed texture shown in Eulerian format.

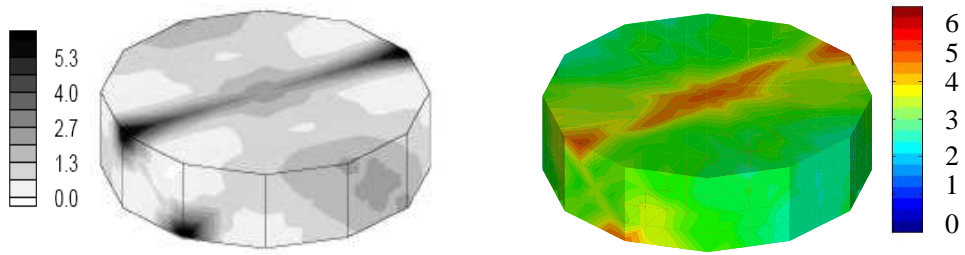


Fig. 5. (left) - Computed texture shown in fundamental space from (Myagchilov and Dawson, 1999); (right) - Computed texture from this work.

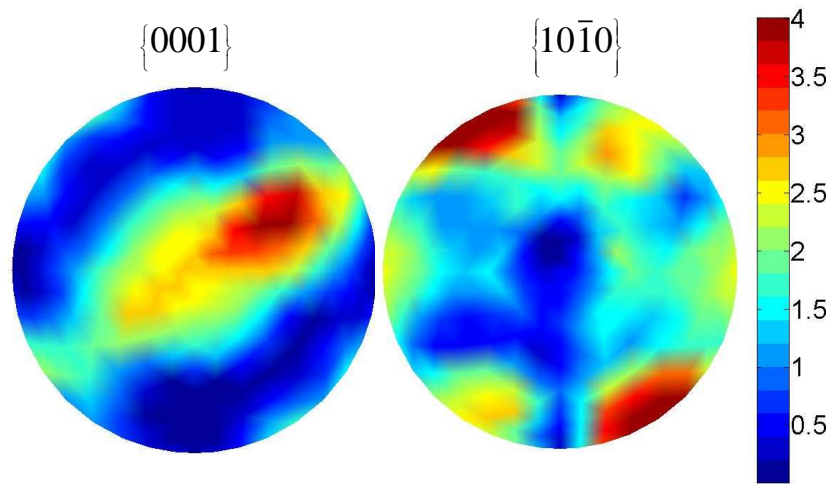


Fig. 6. Computed crystallographic texture in simple shear for  $\alpha$ -Ti at  $\gamma=-1.00$ .

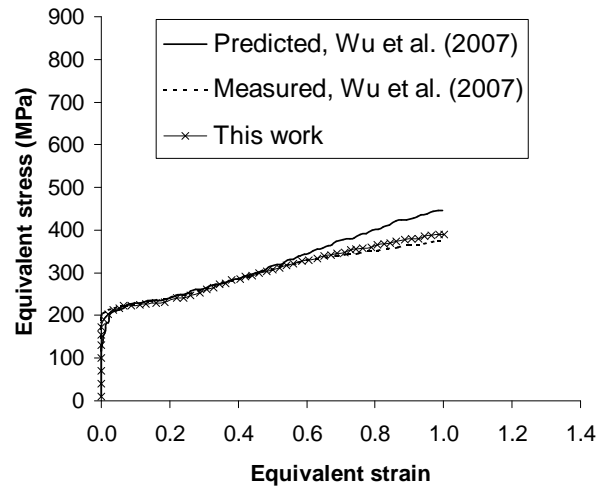


Fig. 7. Comparison between experimentally measured and numerically simulated stress-strain curve (Wu et al., 2007) and the result from this work.

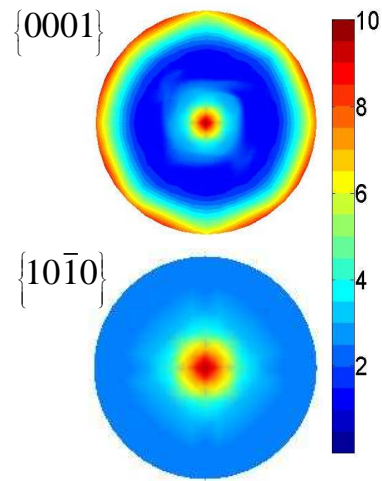


Fig. 8. Initial texture used in this work for Mg.

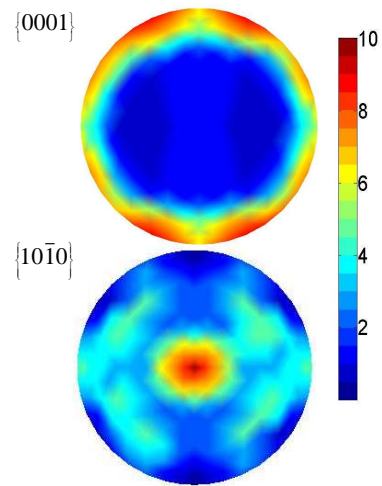


Fig. 9. Computed crystallographic texture in simple tension for the tensile strain of 15%.

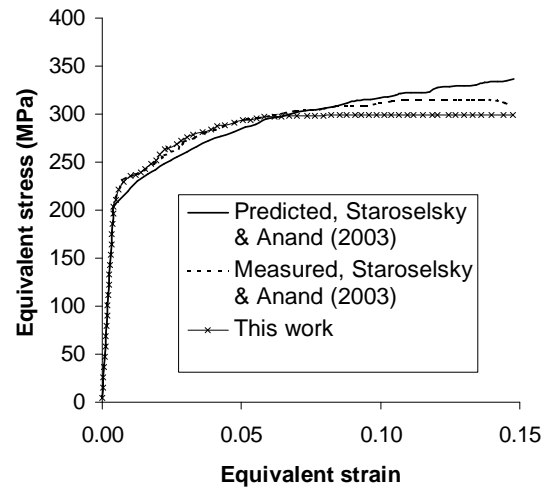


Fig. 10. Comparison between experimentally measured and computed stress-strain response from (Staroselsky and Anand, 2003) and the result from this work.

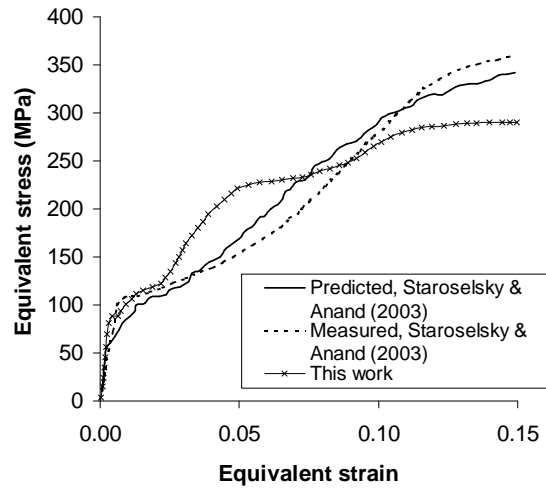


Fig. 11. Comparison between experimentally measured and numerically simulated stress-strain curve (Staroselsky and Anand, 2003) and the result from this work for the simple compression mode.

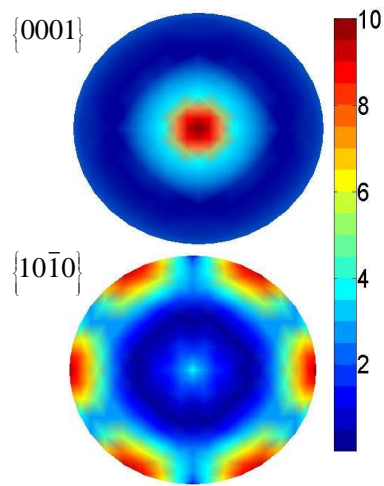


Fig. 12. Numerically simulated crystallographic texture in simple compression for the compressive strain of 18%.

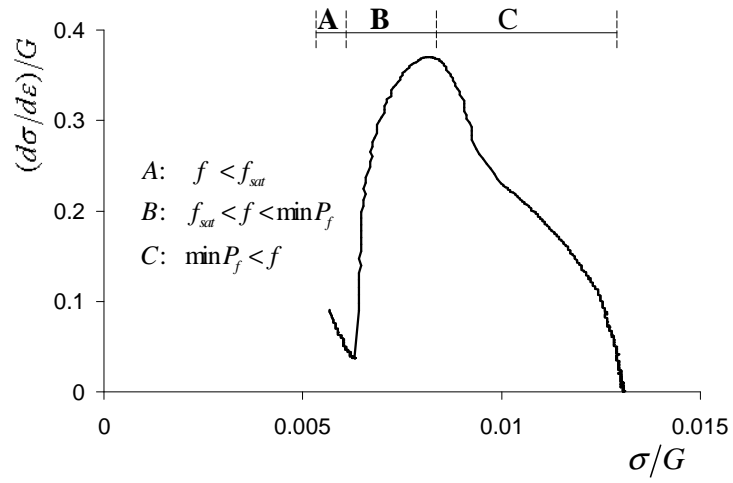


Fig. 13. Normalized strain hardening response of magnesium alloy AZ31B in simple compression. A, B and C represent three different stages.  $f$ ,  $f_{sat}$  and  $P_f$  are defined in Section 5.1.

Table 1  
HCP slip system parameters (Staroselsky and Anand 2003)

Type	Slip plane normal	Slip direction
Basal	$\{0001\}$	$\langle 11\bar{2}0 \rangle$
Prismatic	$\{10\bar{1}0\}$	$\langle 11\bar{2}0 \rangle$
Pyramidal	$\{10\bar{1}1\}$	$\langle 11\bar{2}0 \rangle$
Twin	$\{10\bar{1}2\}$	$\langle \bar{1}011 \rangle$